A Single-Layered Spoof-Plasmon-Mode Leaky Wave Antenna With Consistent Gain

Amin Kianinejad, *Student Member, IEEE*, Zhi Ning Chen, *Fellow, IEEE*, and Cheng-Wei Qiu, *Member, IEEE*

***Abstract*— A single-layered leaky wave antenna (SL-LWA) exploiting the groundless spoof plasmons (SPs) structure is presented and validated to achieve consistent scanning beam and broadside gain across a wide bandwidth. The antenna is composed of single-layered meander SP cells and coplanar waveguide to SP structure converters. The periodically arranged SP cells of the SL-LWA generate a radiating space harmonic with forward, backward, and broadside radiation against frequency change. The study and experimental validation show that the proposed SL-LWA provides the consistent gain variation less than 2.5 dB of scanning beams within the 10-dB reflection bandwidth of 10.4–24.5 GHz (or 80%). In addition, the proposed antenna offers the wideband broadside radiation with 1-dB gain variation within the frequency range of 16.5–17.2 GHz (or 4.2%). The method to design the antenna operating at desired frequencies is provided. Benefiting from the low-profile compactness and unprecedented performance, the proposed SL-LWA has promising potentials for applications in wireless systems.**

***Index Terms*— Antenna radiation patterns, beam steering, leaky wave antennas (LWAs), periodic structures, plasmons.**

I. Introduction

THE radiation from traveling wave structures is first proposed by Hansen [1]. With their nonresonant nature, traveling wave antennas offer unique features, such as wide operating bandwidth, high gain, and frequency beam scanning for the applications in millimeter wave and microwave systems [2]–[4].

Usually, the leaky wave antennas (LWAs) are terminated by a broadband load to absorb the nonradiated power and prevent it from reflecting to the input and disturbing desired radiation patterns. This termination reduces the antenna efficiency, especially at the higher frequencies where the nonradiated power increases. Nguyen *et al.* [5] proposed a power recycling feedback system to solve this issue for maximizing the antenna efficiency. However, this additional power recycling unit increases the total size as well as the total ohmic loss of the antenna.

Manuscript received July 21, 2016; revised October 20, 2016; accepted November 7, 2016. Date of publication November 29, 2016; date of current version February 1, 2017.

A. Kianinejad is with the Department of Electrical and Computer Engineering, National University of Singapore, Singapore 117583, and also with the Institute for Infocomm Research, Agency of Science, Technology and Research, Singapore 138632 (e-mail: amin@nus.edu.sg).

Z. N. Chen and C.-W. Qiu are with the Department of Electrical and Computer Engineering, National University of Singapore, Singapore 117583 (e-mail: eleczn@nus.edu.sg; chengwei.qiu@nus.edu.sg).

Color versions of one or more of the figures in this paper are available online at http://ieeexplore.ieee.org.

Digital Object Identifier 10.1109/TAP.2016.2633161

Among LWAs, planar LWAs have been of more interest due to their low-profile configurations [6]–[10]. Recently, planar LWAs designed by composite right/left handed (CRLH) structures have been proposed to realize the wide bandwidth of consistent broadside gain (4.2%) [11]. This design as well as many other CRLH material-based LWAs require an arrangement of metal patches and via holes with two metallic layers.

Recently, spoof plasmon (SP) modes with their high field confinement, lower leaky and ohmic loss, and flexible planar structures have inspired much research interest in microwave designs, including waveguides[12], transmission lines [13]–[16], frequency splitters [17], and ultrawideband SP filters [18]. The SP modes have also found their way in antenna engineering [19]–[25]. In [21], an array of microstrip patch antennas is fed by an SP-based waveguide. A slow wave feeding method to excite the dominant TE modes of dielectric resonator antennas is proposed in [24]. In [25], additional gaps are implemented between the cells of an SP-based transmission line to convert the slow waves to fast radiating waves, and design an SP-based LWA with fixed radiation patterns.

This paper implements the SP modes to design a single-layered LWA (SL-LWA). With a simple and single layer structure, the proposed design offers all the advantageous features of the conventional LWAs, such as the frequency scanning beam, forward, broadside and backward radiations, and broadband operation for broadside radiation. With the very low nonradiative power at the end of the antenna, the proposed LWA does not need any loading termination. In Section II, the radiation from the proposed monolayer LWA is studied. In Section III, a simple design procedure for the SL-LWA is provided. In Section IV, the radiation performance of the antenna is experimentally evaluated.

II. Radiation Mechanism

The operation principle of the periodic LWAs is based on the generation of a radiating space harmonic [2]. Here, a method to generate the leaky wave mode in the SP-based structures is proposed to design a new type of LWAs.

A. Single-Layered Leaky Wave Antenna

A meander SP cell, presented in Fig. 1(a) (inset), is composed of two reversely attached U-shaped SP units. Compared with the H-shaped SP cells [26], the meander SP is more compact, and in comparison with the single-side U-shaped SP

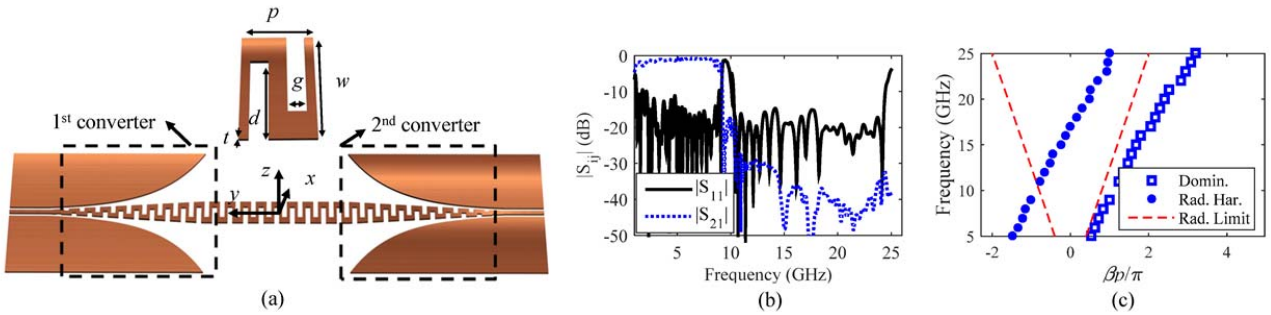

Fig. 1. (a) SW-TL composed of meander SP cells. Inset: meander SP cell. (b) Scattering parameter results from the meander SW-TL. (c) Dispersion curves for the dominant mode and the first space harmonic of the meander SW-TLs.

designs [27], it benefits from a double-sided configuration, which makes it more compatible with the symmetric conventional transmission lines. The geometrical parameters are as follows: the total width is w, groove depth and groove width are d and g, respectively, and the period length is p.

The meander-line slow wave transmission line (SW-TL) is shown in Fig. 1(a) and is composed of periodic meander SP cells connected to coplanar waveguide (CPW) lines via two converters. The converter consists of two parts: a flaring ground to provide a smooth transition from the CPW to the groundless SW-TL. The other part of the converter is the strip connector, which connects the strip of CPW to the SP cells and is composed of several meander cells with the same periodicity and groove width but gradually increasing width and groove depth. The design procedure for the converter is detailed in [24].

The simulation results for the scattering parameters from the designed meander-line SW-TL are presented in Fig. 1(b). The substrate is Rogers 4003 and the geometrical parameters of the cell are $p = 12$ mm, $w = 5$ mm, $d = 2$ mm, and $g = p/2$. As seen, the cut-off frequency for this cell is 9 GHz. For the frequencies below 9 GHz, the transmission is above -0.5 dB; the reflection is below -15 dB, and the meander-line SW-TL operates in the transmission line mode. However, within the range of 9–10.4 GHz, the transmission is suppressed so that no energy is transmitted through the meander SW-TL. Above 10.4 GHz, the reflection decreases while the transmission remains negligible.

The dispersion curves for the two modes in the meander-line SW-TL are shown in Fig. 1(c). These results are calculated by taking the Fourier transform of the waves on the SW-TL at various frequencies. The space harmonic corresponds to the Bloch mode with $n = -1$ and its wavenumber (β_{-1}) is

$$\beta_{-1} = \beta_0 - 2\pi/p \tag{1}$$

where β_0 is the wavenumber of the dominant mode. The red dashed lines in Fig. 1(c) specify the fast wave limit where the wavenumber is lower than the free space wavenumber (k_0). For the frequencies within 10.4–24.5 GHz, where the first space harmonic lies in the radiation range, the reflection decreases while the transmission remains negligible, according to the results in Fig. 1(b). Consequently, the energy leaks from the transmission line and the SW-TL acts as an SL-LWA.

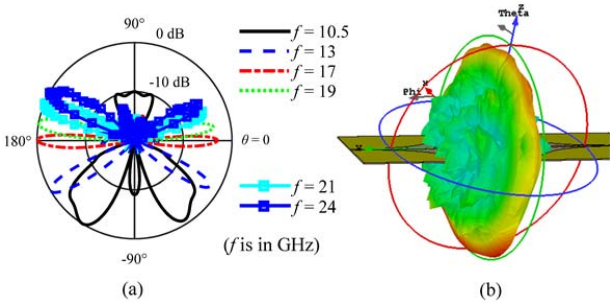

Fig. 2. (a) Normalized cocomponent (φ) radiation patterns of the SL-LWA in the yz plane at frequencies. (b) 3-D radiation pattern of the SL-LWA at 17 GHz simulated by CST Microwave Studio.

The main beam radiation direction can be calculated from the radiating space harmonic dispersion curve as follows:

$$\theta_{\text{main}} = \begin{cases} \text{Arcsin}\left(\dfrac{\beta_{-1}}{k_0}\right) \\ \pi - \text{Arcsin}\left(\dfrac{\beta_{-1}}{k_0}\right). \end{cases} \tag{2}$$

The first angle corresponds to the radiation in the top space while the second angle corresponds to that in the bottom space.

Fig. 2(a) plots the normalized radiation pattern of the SL-LWA for the cocomponent (φ) in yz plane. At 10.5 GHz, the main beam is titled toward $-120°$. As the frequency increases from 10.5 to 17 GHz, the radiation direction changes from backward to broadside radiation. At 17 GHz, the momentum of the radiating space harmonics is equal to zero, as can be seen in Fig. 1(c).

Fig. 2(b) shows the 3-D radiation pattern at this frequency. By increasing the frequency from 17 to 24.5 GHz, the radiation beam moves from broadside to forward direction ($\theta = 30°$). These results are in accordance with (2).

B. SL-LWA Without Second Converter

The scattering parameter results plotted in Fig. 1(b) demonstrate that $|S_{21}|$ of the SL-LWA within the radiation range from $f = 10.4$ to 24.5 GHz is lower than -12 dB. In other words, most of the energy radiates and the transmitted energy to Port 2 is almost zero over the entire bandwidth. This is one of the advantages of this design in comparison with the other types of LWAs, where the transmitted power increases by increasing

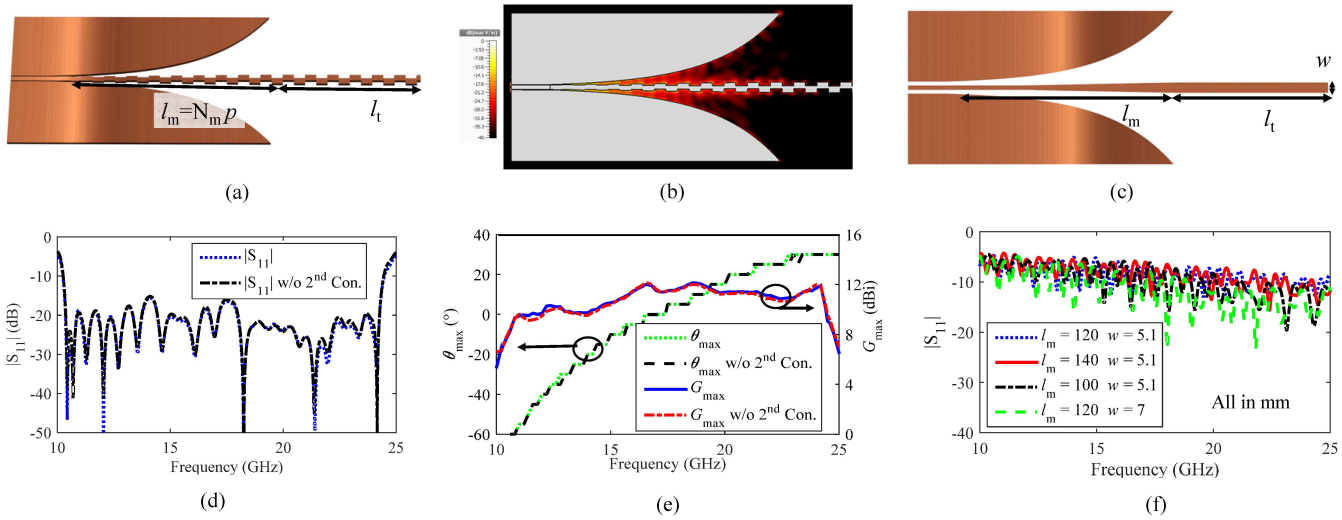

Fig. 3. (a) SL-LWA without the second converter. (b) Electric field distribution near the SL-LWA. (c) Simple strip antenna without grooves. (d) Reflection spectrum. (e) Maximum radiation direction and gain of the SL-LWA for two cases: with and without the second converter. (f) Reflection results from the simple stipe for various geometrical parameters.

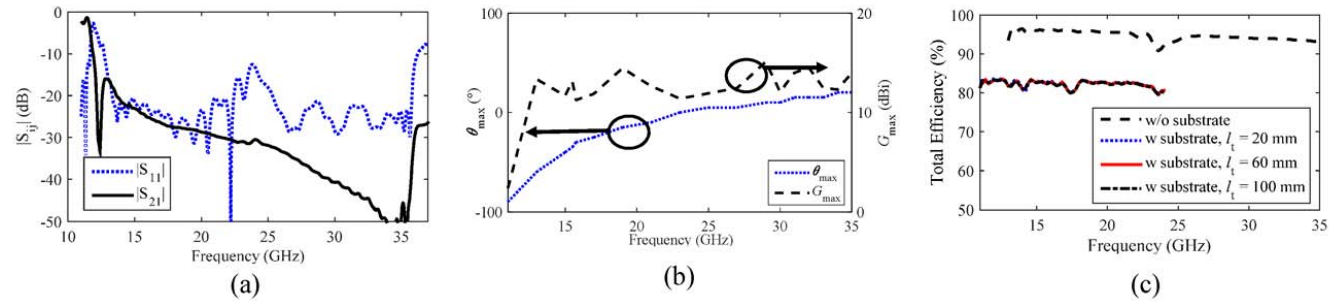

Fig. 4. (a) Scattering parameter results from the SL-LWA without the dielectric substrate. (b) Maximum radiation angle and the gain of the SL-LWA without the dielectric substrate. (c) Total efficiency of the SL-LWA with and without the dielectric substrate for various l_t.

the frequency and the radiation efficiency of the antenna drops significantly at higher frequencies.

The SL-LWA is composed of two converters [see Fig. 1(a)]. To study the effect of the second converter on the radiation, this part is removed [see Fig. 3(a)], and for the two cases with and without the second converter, the reflection spectrum and radiation performance are compared in Fig. 3(d) and (e), respectively. This results show that removing the second converter does not affect the reflected power, radiation angle, and maximum gain, that is, the majority of the power has been radiated before reaching the second converter in Fig. 1(b). Moreover, it can be concluded that without any loading termination for the SL-LWA, the performance of the antenna keeps unchanged.

C. Comparison With Other LW Structures Similar to SL-LWA

The SL-LWA is composed of the SP cells as well as the flaring ground. The periodic cells are responsible for the generation of the space harmonics and radiating the EM energy. The flaring ground converts the CPW modes to the SP modes and has no significant effect on the radiation. Fig. 3(b) shows the field distribution of the SL-LWA at 17 GHz. These results demonstrate that the majority of the electromagnetic energy is distributed near the meander strip, while this distribution is negligible near the flaring ground.

To further study the effect of the grooves on the antenna operation, a structure similar to Fig. 3(a) without grooves is simulated, as shown in Fig. 3(c). The reflection spectrum is shown in Fig. 3(f) for varying geometrical parameters. These results indicates that the flaring ground along with the central conducting strip without grooves could not generate the wideband radiation for any of the parameter sets and this structure could not operate as a wideband antenna.

The flaring ground of the SL-LWA may also resemble a tapered slot antenna (TSA) [28], [29]. While this part of the SL-LWA does not radiate, the flared slot in TSAs radiates the electromagnetic energy and generates a fixed endfire beam, which is different from the frequency scanning radiating beam of the SL-LWA. These two kinds of radiation patterns suggest that the radiation mechanisms of these two types of antennas are different from each other.

D. Dielectric and Metal Effect

To study the effect of the dielectric substrate on the radiation performance of the SL-LWA, the antenna without the substrate is simulated and compared with the same antenna on the substrate. Fig. 4(a) shows the scattering parameters of the LWA without supporting dielectric. As seen, removing the substrate shifts the operation frequency to 12.7–35 GHz and increases the bandwidth from 80% to 94%. We removed the

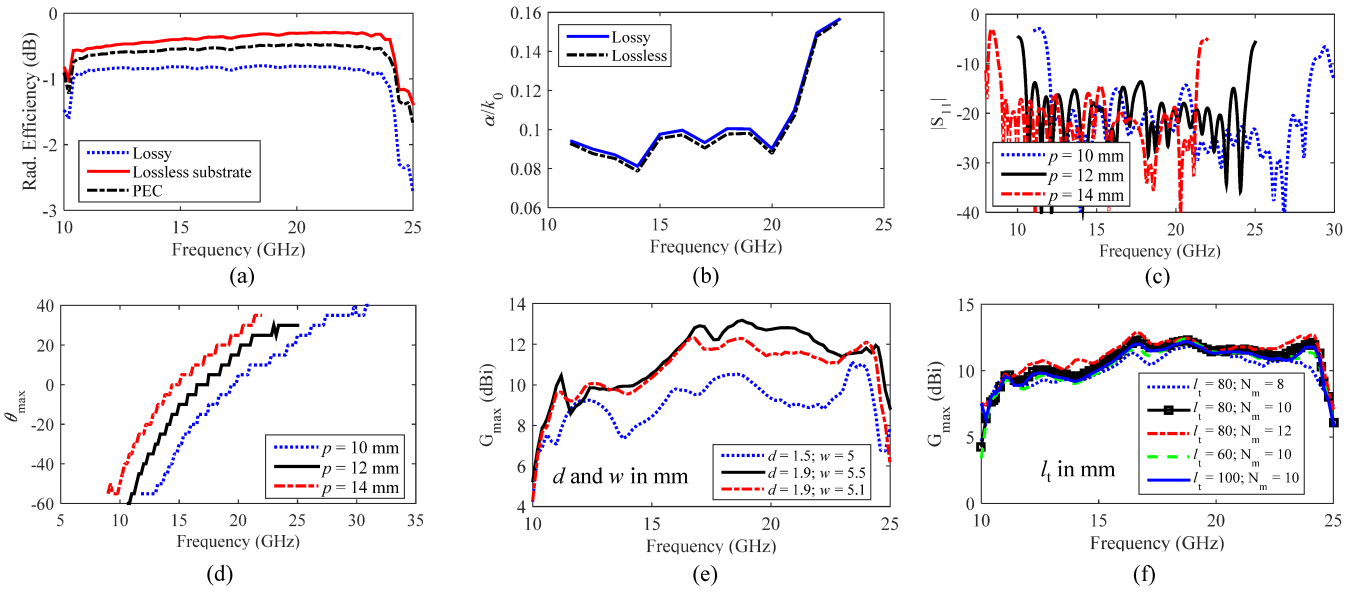

Fig. 5. (a) Radiation efficiency of the SL-LWA for three cases: SL-LWA with lossy metal and dielectric, SL-LWA with lossless dielectric, and SL-LWA with PEC as metal. (b) Normalized decay rate of the SL-LWA. (c) Reflection spectrum results. (d) Maximum radiation direction and (e) gain of the SL-LWAs with varying geometrical parameters. (f) Maximum gain for SL-LWA with varying N_m and l_t.

second converter of the SL-LWA without dielectric, similar to Fig. 3(a), and studied the radiation performance of the antenna. The maximum radiation angle and the maximum gain in the yz plane are shown in Fig. 4(b).

Fig. 4(c) compares the total efficiency of the SL-LWA with and without the substrate. For the SL-LWA with substrate, three cases are compared with different l_t values [see Fig. 3(a)]. Without considering the dielectric loss, the antenna efficiency is around 95% for the entire frequency range. Fig. 4(c) shows that at 23.6 GHz, the efficiency drops to 90%. At this frequency, the main beam points at $\theta = 0°$ and the radiation is broadside [see Fig. 4(b)]. The slight reduction of the antenna efficiency is due to the slight increase of the reflection at the broadside frequency, according to Fig. 4(a). However, the antenna efficiency is above 90% over the entire bandwidth, which shows the excellent radiation performance of the SL-LWA without the substrate. Considering the 1.5-mm-thick Rogers 4003 substrate, the efficiency reduces to 82%. The antenna efficiency is reduced, because the substrate introduces the additional dielectric loss to the antenna. Effect of the antenna length is also studied in Fig. 4(c). These results indicate that changing l_t does not affect the total antenna efficiency significantly. However, this parameter affects the antenna gain and is studied in Section III.

To further study the effect of the ohmic losses caused by dielectric and metal on the antenna performance, the radiation efficiency of the SL-LWA for three cases is studied in Fig. 5(a): 1) SL-LWA with lossy metal and on lossy substrate tagged as "lossy;" 2) SL-LWA with lossy metal and on lossless substrate tagged as "lossless substrate;" and 3) SL-LWA with PEC as metal and on lossy substrate tagged as "PEC." Fig. 5(a) shows that the effect of the metal loss on the radiation efficiency is less than that by the dielectric loss. In addition, both losses reduce the efficiency about 1 dB for the entire bandwidth.

Fig. 5(b) plots the normalized attenuation constant of the fields of the SL-LWA for both the two cases of lossy and lossless antennas. Fig. 5(b) shows that even for the SL-LWA with lossless materials, the fields attenuate and the structure operates as an efficient LWA. The performance of conventional LWAs usually degrades by increasing the frequency because of the increased forward transmission as the frequency increases. In contrast, the proposed design offers an almost consistent performance for the entire frequency range.

III. Design Procedure and Optimization

It is important to design the SL-LWA for the operation at the desired frequency. One way is to tune the dispersion curve of the radiating space harmonic and shift it to other frequency ranges. By increasing and decreasing the periodicity, the dispersion line of this harmonic in Fig. 1(c) moves right and left, respectively. Fig. 1(c) indicates a linear dispersion curve. In other words, operating at the dominant mode, the SL-LWA can be approximated by a medium with an effective permittivity of $\varepsilon_{\text{eff}} = 2.2$. Our simulation for SL-LWAs shows that above the cut-off frequency and within the leaky wave frequency range, the effective permittivity of the dominant mode only depends on the substrate permittivity and its thickness and does not change significantly by changing the geometrical parameters of the SP cells. Consequently, according to (2), the space harmonic follows the following dispersion relation:

$$\beta_{-1} = \sqrt{\varepsilon}_{\text{eff}} k_0 - \frac{2\pi}{p}. \tag{3}$$

For the meander cell studied in Fig. 1(c), p is set as 12 mm and the broadside radiation ($\beta_{-1} \simeq 0$) occurs at 17 GHz. According to (3), to achieve broadside radiation at 14.5 and 20 GHz, the periodicity (p) should be chosen as 14 and 10 mm, respectively. Fig. 5(c) and (d) demonstrates

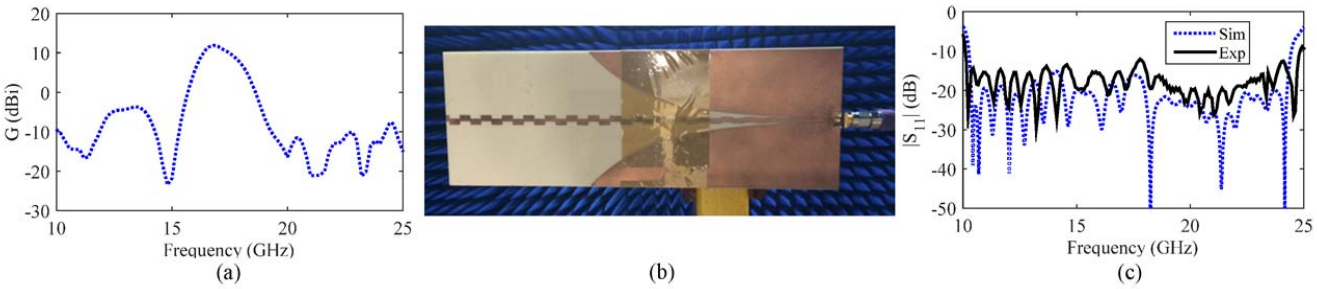

Fig. 6. (a) Broadside gain of the SL-LWA over the frequency range. (b) Fabricated SL-LWA. (c) Measured reflection spectrum compared with the simulation results.

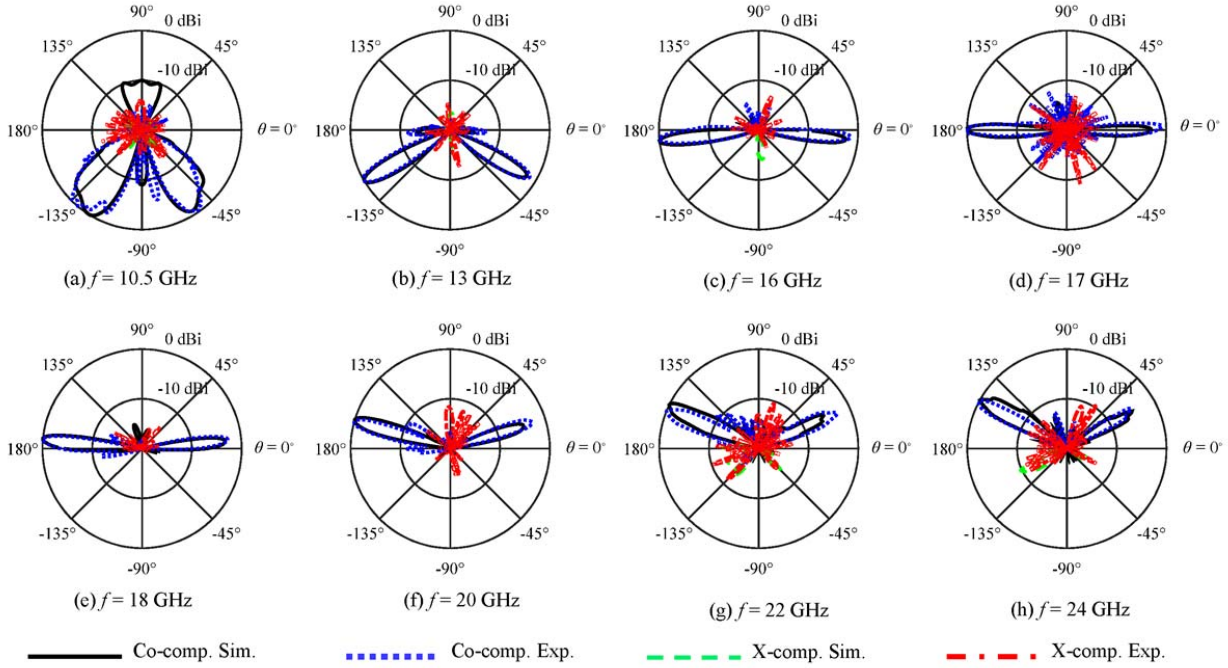

Fig. 7. Comparison between the measured and simulated results for the normalized radiation pattern of the SL-LWA for the cocomponent (φ) as well as cross-component (θ) in the yz plane at (a) 10.5, (b) 13, (c) 16, (d) 17, (e) 18, (f) 20, (g) 22, and (h) 24 GHz.

the effects of the periodicity (p) on the operating bandwidth and radiation angle, respectively. As p increases, the operating frequency range shifts to lower frequencies while the bandwidth is kept as 80%. Consequently, the radiation angle curve shifts to lower frequencies while the scanning range remains constant. The broadside radiation frequency also corresponds to $f = 14.5$ and 20 GHz, as were calculated from (3).

Fig. 5(e) shows the maximum gain of the φ-component in the yz plane for the three sets of parameters. For $d = 1.9$ mm and $w = 5.1$ mm, the most consistent as well as highest gain over the frequency are achieved. The other parameters that can be tuned are the length of the converter ($l_m = N_m p$) and l_t [see Fig. 3(a)]. Fig. 5(f) plots the maximum gain of the φ-component in the yz plane for varying l_t and N_m. Among all the parameters studied in Fig. 5(f), the selection of $N_m = 10$ and $l_t = 80$ mm achieves the most consistent gain over the frequency range and is chosen for prototyping.

Fig. 6(a) plots the broadside realized gain over the frequency range. Fig. 6(a) indicates that the operation band for less than 1-dB gain variation is 16.5–17.2 GHz or 4.2%. Benefiting from a single layer and planar configuration, the proposed LWA offers its broadband operation with a consistent broadside gain comparable with previous designs.

IV. Experimental Verification

The designed SL-LWA was fabricated and experimentally validated [see Fig. 6(b)]. The reflection from the antenna was measured using a vector network analyzer and compared with the simulation results in Fig. 6(c). Both results match well and demonstrate the good matching over a wide frequency range from 10.4 to 24.5 GHz. The measured $|S_{11}|$ is slightly higher than the simulated values, maybe caused by the SMA connector, which was not considered in the simulation.

The radiation patterns were measured in an anechoic chamber. As the operating frequency range of the power amplifier (PA) in the measurement setup was limited, the measurement was performed for the two frequency ranges of 10.5–18 and 18–24.5 GHz separately with two different PAs. For the higher frequency range, two low noise amplifiers

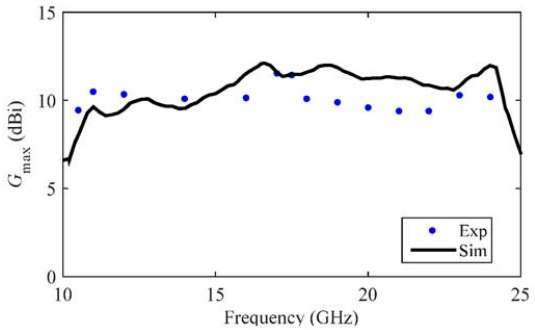

Fig. 8. Comparison between the measured and simulated results for the maximum realized gain of the SL-LWA in the *yz* plane.

were used before the transmit antenna as well as after the antenna under the test to compensate for the higher loss at higher frequencies and keep the measured results above the noise floor of the network analyzer.

The normalized radiation patterns in the *y*z plane are compared with the simulation results in Fig. 7. The cross-polarized component (θ) is at least 12 dB lower than the copolarized component (φ) at all the frequencies and all the angles. The experimental results match well the simulation and demonstrate the sweep of the main beam by changing the frequency. According to Fig. 1(c), the momentum of the first space harmonic at 17 GHz is zero, which corresponds to the broadside radiation, as it can be seen in Fig. 7(d). For the frequencies lower than 17 GHz, β_{-1} is smaller than 0, which corresponds to the backward radiation [see Fig. 7(a)–(c)]. As the frequency increases, β_{-1} increases and the main beam tilts to the forward direction [see Fig. 7(e)–(h)].

The gain in the maximum radiation direction at various frequencies was measured and compared with the simulation results in Fig. 8. A good agreement is observed between the results. The gain variation across the entire bandwidth is limited to 2.5 dB. The constant gain is an important advantage of the proposed LWA over the conventional LWAs with dropping gain at the broadside and/or forward radiation. At 17 GHz, where the radiation is in broadside, the gain is as high as the rest of the bandwidth and no gain reduction can be observed.

V. Conclusion

An SL-LWA based on meander SP cells has been designed and experimentally verified. The proposed antenna has achieved a wide operating bandwidth of 80% with high and consistent total efficiency, gain, and a wideband broadside radiation over 4.2% bandwidth. The reflection bandwidth has been up to 95%. With the unique simple design free of ground planes and via holes, the SL-LWAs pave the avenue for the applications of LWAs in integrated microwave circuits.

References

[1] W. W. Hansen, "Radiating electromagnetic wave guide," Google Patent 2 402 622, Jun. 25, 1946.

[2] D. R. Jackson, C. Caloz, and T. Itoh, "Leaky-wave antennas," *Proc. IEEE*, vol. 100, no. 7, pp. 2194–2206, Jul. 2012.

[3] J. L. Gómez-Tornero, A. la Torre Martínez, D. C. Rebenaque, M. Gugliemi, and A. Álvarez-Melcón, "Design of tapered leaky-wave antennas in hybrid waveguide-planar technology for millimeter wave-band applications," *IEEE Trans. Antennas Propag.*, vol. 53, no. 8, pp. 2563–2577, Aug. 2005.

[4] F. Xu, K. Wu, and X. Zhang, "Periodic leaky-wave antenna for millimeter wave applications based on substrate integrated waveguide," *IEEE Trans. Antennas Propag.*, vol. 58, no. 2, pp. 340–347, Feb. 2010.

[5] H. V. Nguyen, A. Parsa, and C. Caloz, "Power-recycling feedback system for maximization of leaky-wave antennas' radiation efficiency," *IEEE Trans. Microw. Theory Techn.*, vol. 58, no. 7, pp. 1641–1650, Jul. 2010.

[6] Y.-D. Lin and J. Sheen, "Mode distinction and radiation-efficiency analysis of planar leaky-wave line source," *IEEE Trans. Microw. Theory Techn.*, vol. 45, no. 10, pp. 1672–1680, Oct. 1997.

[7] Y. Dong and T. Itoh, "Substrate integrated composite right-/left-handed leaky-wave structure for polarization-flexible antenna application," *IEEE Trans. Antennas Propag.*, vol. 60, no. 2, pp. 760–771, Feb. 2012.

[8] L. Liu, C. Caloz, and T. Itoh, "Dominant mode leaky-wave antenna with backfire-to-endfire scanning capability," *Electron. Lett.*, vol. 38, no. 23, pp. 1414–1416, Nov. 2002.

[9] A. Alu, F. Bilotti, N. Engheta, and L. Vegni, "Subwavelength planar leaky-wave components with metamaterial bilayers," *IEEE Trans. Antennas Propag.*, vol. 55, no. 3, pp. 882–891, Mar. 2007.

[10] S. K. Podilchak, A. P. Freundorfer, and Y. M. M. Antar, "Planar leaky-wave antenna designs offering conical-sector beam scanning and broadside radiation using surface-wave launchers," *IEEE Antennas Wireless Propag. Lett.*, vol. 7, pp. 155–158, 2008.

[11] N. Nasimuddin, Z. N. Chen, and X. Qing, "Substrate integrated metamaterial-based leaky-wave antenna with improved boresight radiation bandwidth," *IEEE Trans. Antennas Propag.*, vol. 61, no. 7, pp. 3451–3457, Jul. 2013.

[12] M. Navarro-Cía, M. Beruete, S. Agrafiotis, F. Falcone, M. Sorolla, and S. A. Maier, "Broadband spoof plasmons and subwavelength electromagnetic energy confinement on ultrathin metafilms," *Opt. Exp.*, vol. 17, no. 20, pp. 18184–18195, 2009.

[13] D. Martin-Cano, O. Quevedo-Teruel, E. Moreno, L. Martin-Moreno, and F. J. Garcia-Vidal, "Waveguided spoof surface plasmons with deep-subwavelength lateral confinement," *Opt. Lett.*, vol. 36, no. 23, pp. 4635–4637, 2011.

[14] M. Navarro-Cía, M. Beruete, M. Sorolla, and S. A. Maier, "Enhancing the dual-band guiding capabilities of coaxial spoof plasmons via use of transmission line concepts," *Plasmonics*, vol. 6, no. 2, pp. 295–299, 2011.

[15] A. Kianinejad, Z. N. Chen, and C.-W. Qiu, "Design and modeling of spoof surface plasmon modes-based microwave slow-wave transmission line," *IEEE Trans. Microw. Theory Techn.*, vol. 63, no. 6, pp. 1817–1825, Jun. 2015.

[16] A. Kianinejad, Z. N. Chen, and C.-W. Qiu, "Design and modeling of low-loss symmetric slow-wave transmission lines," in *Proc. Asia–Pacific Microw. Conf. (APMC)*, Dec. 2015, pp. 1–3.

[17] X. Gao *et al.*, "Ultrathin dual-band surface plasmonic polariton waveguide and frequency splitter in microwave frequencies," *Appl. Phys. Lett.*, vol. 102, no. 15, p. 151912, 2013.

[18] X. Gao, L. Zhou, Z. Liao, H. F. Ma, and T. J. Cui, "An ultra-wideband surface plasmonic filter in microwave frequency," *Appl. Phys. Lett.*, vol. 104, no. 19, p. 191603, 2014.

[19] H. Shi, X. Wei, Z. Zhao, X. Dong, Y. Lu, and C. Du, "A new surface wave antenna-based spoof surface plasmon mechanism," *Microw. Opt. Technol. Lett.*, vol. 52, no. 10, pp. 2179–2183, Jul. 2010.

[20] O. Quevedo-Teruel, "Controlled radiation from dielectric slabs over spoof surface plasmon waveguides," *Prog. Electromagn. Res.*, vol. 140, pp. 169–179, Aug. 2013.

[21] H. Yi, S.-W. Qu, and X. Bai, "Antenna array excited by spoof planar plasmonic waveguide," *IEEE Antennas Wireless Propag. Lett.*, vol. 13, pp. 1227–1230, 2014.

[22] S.-H. Kim *et al.*, "Subwavelength localization and toroidal dipole moment of spoof surface plasmon polaritons," *Phys. Rev. B*, vol. 91, no. 3, p. 035116, Jan. 2015.

[23] B. Xu *et al.*, "Tunable band-notched coplanar waveguide based on localized spoof surface plasmons," *Opt. Lett.*, vol. 40, no. 20, pp. 4683–4686, 2015.

[24] A. Kianinejad, Z. N. Chen, L. Zhang, W. Liu, and C.-W. Qiu, "Spoof plasmon-based slow-wave excitation of dielectric resonator antennas," *IEEE Trans. Antennas Propag.*, vol. 64, no. 6, pp. 2094–2099, Jun. 2016.

[25] A. Kianinejad, Z. N. Chen, and C.-W. Qiu, "Spoof surface plasmon-based leaky wave antennas," presented at the Asia–Pacific Microw. Conf. (APMC), Delhi, India, Dec. 2016.
[26] H. F. Ma, X. Shen, Q. Cheng, W. X. Jiang, and T. J. Cui, "Broadband and high-efficiency conversion from guided waves to spoof surface plasmon polaritons," *Laser Photon. Rev.*, vol. 8, no. 1, pp. 146–151, 2013.
[27] X. Shen, T. J. Cui, D. Martin-Cano, and F. J. Garcia-Vidal, "Conformal surface plasmons propagating on ultrathin and flexible films," *Proc. Nat. Acad. Sci. USA*, vol. 110, no. 1, pp. 40–45, 2013.
[28] R. Janaswamy and D. H. Schaubert, "Analysis of the tapered slot antenna," *IEEE Trans. Antennas Propag.*, vol. 35, no. 9, pp. 1058–1065, Sep. 1987.
[29] K. S. Yngvesson, T. L. Korzeniowski, Y.-S. Kim, E. L. Kollberg, and J. F. Johansson, "The tapered slot antenna-a new integrated element for millimeter-wave applications," *IEEE Trans. Microw. Theory Techn.*, vol. 37, no. 2, pp. 365–374, Feb. 1989.

Amin Kianinejad (S'14) received the B.Sc. degree in electrical engineering from the Shiraz University of Technology, Shiraz, Iran, in 2008, and the M.Sc. degree in electrical engineering from Sharif University, Tehran, Iran, in 2010. He is currently pursuing the Ph.D. degree with the National University of Singapore, Singapore.

His current research interests include microwave plasmonics, antennas, and metamaterials.

Zhi Ning Chen (M'99–SM'05–F'07) received the B.Eng., M.Eng., and Ph.D. degrees in electrical engineering from the Institute of Communications Engineering (ICE), Nanjing, China, and the Ph.D. degree from the University of Tsukuba, Ibaraki, Japan.

From 1988 to 1995, he was with ICE as a Lecturer and later as an Associate Professor, and with Southeast University, Nanjing, China, as a Post-Doctoral Fellow and later as an Associate Professor. From 1995 to 1997, he was with the City University of Hong Kong, Hong Kong, as a Research Assistant and later became a Research Fellow. In 2001 and 2004, he visited the University of Tsukuba under the Japan Society for the Promotion of Science (JSPS) Fellowship Program (Senior Level). In 2004, he joined the IBM T. J. Watson Research Center, Yorktown Heights, NY, USA, as an Academic Visitor. From 1999 to 2012, he was with the Institute for Infocomm Research (I2R), Singapore, as a Member of Technical Staff (MTS), a Senior MTS, a Principal MTS, a Senior Scientist, a Lead Scientist, a Principal Scientist, and the Head of the RF and Optical Department. In 2012, he joined the Department of Electrical and Computer Engineering, National University of Singapore, Singapore, as a Full Professor. In 2013, he joined the Laboratoire des SignauxetSystèmes, UMR8506 CNRS-Supelec-University Paris Sud, Gif-sur-Yvette, France, as a Senior DIGITEO Guest Scientist. He is concurrently holding a joint appointment as an Advisor and a Principle Scientist with I2R, and Professorships with Southeast University as a Changjiang Guest Professor, with Nanjing University, Nanjing, as a Guest Professor, with Shanghai Jiaotong University, Shanghai, China, as a Guest Professor, with Tsinghua University, Beijing, China, as a Visiting Professor, with Tongji University, Shanghai, as a Guest Professor, with the University of Science and Technology of China, Hefei, China, as a Guest Professor, with Fudan University, Shanghai, as an Outstanding Overseas Visiting Professor, with Dalian Maritime University, Dalian, China, with Chiba University, Chiba, Japan, as a Visiting Professor, with the National Taiwan University of Science and Technology, Taipei, Taiwan, as a Visiting Professor, with Shanghai University, Shanghai, as a Ziqiang Professor, with the Beijing University of Posts and Telecommunications, Beijing, as a Visiting Professor, with Tohoku University, Sendai, Japan, as a Visiting Professor, and with the City University of Hong Kong, Hong Kong, as an Adjunct Professor. He has authored 480 technical papers and authored or edited the books *Broadband Planar Antennas* (Wiley, 2005), *UWB Wireless Communication* (Wiley, 2006), *Antennas for Portable Devices* (Wiley, 2007), and *Antennas for Base Stations in Wireless Communications* (McGraw-Hill, 2009). He has also contributed the chapters to the books *UWB Antennas and Propagation for Communications, Radar, and Imaging* (Wiley, 2006), Antenna Engineering Handbook (McGraw-Hill, 2007), and *Microstrip and Printed Antennas* (Wiley, 2010). He holds 30 granted and filed patents with 31 licensed deals with industry. His current research interest includes electromagnetic engineering, antennas for microwaves, mm-wave, sub-mm-wave, terahertz communication, radar, imaging, and sensing systems.

Dr. Chen was a recipient of the International Symposium on Antennas and Propagation Best Paper Award 2010, the CST University Publication Award 2008, the IEEE AP-S Honorable Mention Student Paper Contest 2008, the Institution of Engineers Singapore Prestigious Engineering Achievement Awards 2006, 2013, and 2014, the I2R Quarterly Best Paper Award 2004, the IEEE International Workshop on Antenna Technology (iWAT) 2005 Best Poster Award, and several technology achievement awards from China from 1990 to 1997. In 1997, he was a recipient of the JSPS Fellowship to conduct his research at the University of Tsukuba. He has been the founding General Chairs of iWAT, the International Symposium on InfoComm and Media Technology in Bio-Medical and Healthcare Applications, the International Microwave Forum, and the Asia-Pacific Conference on Antennas and Propagation. He has been serving the IEEE Antennas and Propagation Society as a Distinguished Lecturer since 2009. He is currently an Associate Editor of the IEEE TRANSACTIONS ON ANTENNAS AND PROPAGATION and Chief Editor of the *Handbook of Antenna Technologies* (Springer References).

Cheng-Wei Qiu (S'03–M'08) received the B.Eng. degree in applied electromagnetics from the University of Science and Technology of China, Hefei, China, in 2003, and the Ph.D. degree in electromagnetic wave theory for complex media from the National University of Singapore (NUS), Singapore, in 2008.

He was a Post-Doctoral Fellow with the Physics Department, specialization in transformation electromagnetics and metamaterials, Massachusetts Institute of Technology, Cambridge, MA, USA, until 2009. In 2009, he joined NUS, as an Assistant Professor. He has held or is holding Visiting Professor positions with the University of Paris 11, Orsay, France, the King Abdullah University of Science and Technology, Saudi Arabia, and Shenzhen University, Shenzhen, China. He has authored over 100 journal peer-reviewed papers and given three keynote presentations in international conferences. His current research interests include electromagnetic wave theory of transformation optic metamaterials, light-matter interaction, and nanophotonics.

Dr. Qiu was a recipient of the SUMMA Graduate Fellowship in Advanced Electromagnetics in 2005, the IEEE Antennas and Propagation Society Graduate Research Award in 2006, the URSI Young Scientist Award in 2008, the NUS Young Investigator Award in 2011, the MIT TR35@Singapore Award in 2012, the Young Scientist Award from the Singapore National Academy of Science 2013, and the Faculty Young Research Award in NUS 2013. He has been the Topical Editor of the *Journal of the Optical Society of America B* since 2016. He has served on the editorial boards for various journals and as the TPC Chairman for various conferences.